論文 / 著書情報
Article / Book Information

Title	Modified-Weibull-stress-based evaluation of brittle fracture occurrence during earthquakes in steel members
Author(s)	Hiroshi Tamura, Eiichi Sasaki, Satoshi Tominaga
Citation	Engineering Fracture Mechanics, Volume 202, pp. 375-393
Pub. date	2018, 10
DOI	http://dx.doi.org/10.1016/j.engfracmech.2018.08.005
Creative Commons	See next page.
Note	This file is author (final) version.

License

Engineering Fracture Mechanics xxx (xxxx) xxx–xxx

Contents lists available at ScienceDirect

Engineering Fracture Mechanics

journal homepage: www.elsevier.com/locate/engfracmech

Modified-Weibull-stress-based evaluation of brittle fracture occurrence during earthquakes in steel members

H. Tamura[a,*], E. Sasaki[a], S. Tominaga[b]

[a] Department of Civil and Environmental Engineering, School of Environment and Society, Tokyo Institute of Technology, 2-12-1-M1-23, Ookayama, Meguro-ku, Tokyo, Japan

[b] Graduate School of Science and Engineering, Tokyo Institute of Technology, 2-12-1-M1-23, Ookayama, Meguro-ku, Tokyo, Japan

ABSTRACT

Brittle fractures can originate from shallow surface cracks on welded parts of steel structures during earthquakes. Since the occurrence of such fractures is significantly influenced by the shape of the welded parts, the existing methods based on material testing cannot predict fractures. This study focused on a modified Weibull stress, which considers the processes of nucleation and propagation of microcracks at different depths, and demonstrated its applicability to the evaluation of brittle fracture initiation during earthquakes. The demonstration was implemented on three types of structural steel using low-temperature experiments and numerical stress analyses on crack tips. Additionally, the independency of the obtained critical modified Weibull stress from the initial crack depth, strain rate and prestrain was examined in the prediction of the critical crack-tip opening displacement. Finally, the relationship between the critical deformation of the beam-to-column connection of a steel bridge pier at the fracture time (in the case of a fracture originating from a shallow crack) and its weld toe radius was quantitatively evaluated as an example of actual use of the modified-Weibull-stress-based evaluation.

1. Introduction

During the Northridge Earthquake in 1994 and Kobe Earthquake in 1995, brittle fractures initiating at the weld joints were observed in a number of steel structures as shown in Fig. 1 [1–3]. This represented a big issue since this type of fracture, hereafter referred to as brittle fracture during earthquakes, had never been observed before.

The initiation process of brittle fracture during earthquakes is divided into three phases:

Phase 1: Crack initiation at weld parts (ductile or low-cycle fatigue cracks).
Phase 2: Stable propagation of the crack.
Phase 3: Sudden transfer to unstable propagation caused by cleavage fracture of steel.

The effects of plastic strain history and multiaxial stress state on crack initiation [4–9], and of plastic strain history and high strain rate on fracture toughness deterioration involved in cleavage fracture [10–13] have been investigated, and this research has revealed the fundamental nature of the fracture. It is accepted that plastic strain history, multiaxial stress state and high strain rate are the unique factors of brittle fracture during earthquakes, in contrast to widely-known factors such as low temperature, low fracture toughness at heat affected zone, hydrogen embrittlement, etc., that govern brittle fractures.

Another aspect of brittle fractures during earthquakes is the critical condition for cleavage fracture of steel. A shallow ductile crack with a critical depth of about 0.7 mm was observed to be the initial crack of a brittle fracture of a steel bridge pier damaged during the Kobe Earthquake. This suggests that as a result of significant reduction in fracture toughness, mainly caused by severe

* Corresponding author.
E-mail address: tamura.h.ad@m.titech.ac.jp (H. Tamura).

https://doi.org/10.1016/j.engfracmech.2018.08.005
Received 26 August 2017; Received in revised form 26 July 2018; Accepted 3 August 2018

Nomenclature

a_0	initial crack depth
c_0	initial crack width
dV	infinitesimal volume used in the integration of MWS over V_p
E	Young's modulus
m	Weibull shape parameter
N, n	size of data set
N_0	initial number of carbides
N_{unc}	number of uncracked carbides
p_{nucl}	local probability of microcrack nucleation
p_{propag}	local probability of microcrack propagation
P_{cleav}	local cleavage probability
P_{cr}	critical load measured in experiments
P_f	global cleavage probability
R_{notch}	notch radius of the specimens
R_{toe}	weld bead toe radius of the fracture origin
T_0	reference temperature
U_{cr}	critical measured displacement of fixtures in experiments
V_0	elementary volume of Vp
V_p	volume of the fracture process zone
α	plastic strain sensitivity of p_{nucl}
α_0	reference plastic strain sensitivity
δ	crack-tip opening displacement (CTOD)
δ_{cr}	critical CTOD
Δ	displacement of beam-to-column connections (BCC displacement)
Δ_{cy}	critical BCC displacement
Δ_y	BCC displacement at the yield point
ε^p	equivalent plastic strain
ε_0^p	reference plastic strain
ε_u^p	value of ep in dV at the loading history point for which MWS is calculated
$\dot{\varepsilon}^p$	equivalent plastic strain rate
σ_1	maximum principal stress
σ_{th}	threshold critical stress
σ_u, σ_u^*	Weibull scaling parameters for conventional and modified Weibull stress model
σ_w, σ_w^*	conventional and modified Weibull stress (WS and MWS)
$\sigma_{w,cr}$, $\sigma_{w,cr}^*$	critical WS and MWS (CWS and CMWS)
σ_{ys}	yield strength
$\sigma_{ys,0}$	reference yield strength

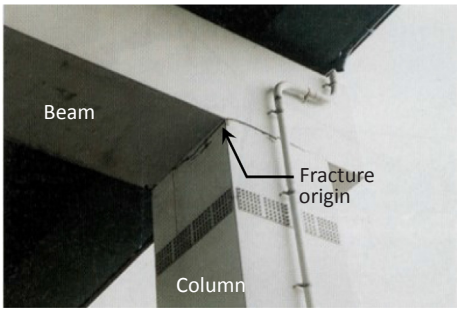

Fig. 1. Example of damage caused by brittle fracture during the Kobe earthquake, which occurred in a rigid-frame pair.

plastic strain history, cleavage fractures in real structures might occur from very shallow cracks during earthquakes.

In cleavage fractures triggered by shallow cracks, not only the crack tip plastic constraint changes with crack depth but also the surface geometry, such as the weld toe, affects the critical condition for cleavage fracture. For instance, the critical Weibull stress (CWS) proposed by Beremin [14] in a specimen evaluated in WES2808 [15] demonstrated an inconvenient dependency on the crack depth and notch radius in the case of fractures from a shallow crack with a depth of less than about 1.0 mm [16]. Tamura et al. [16] also experimentally showed that the Weibull stress (WS) is inadequate to predict cleavage fracture from very shallow cracks since in those cases the fracture is observed during a reduction of the WS, while the WS was previously regarded as a factor driving cleavage fracture. This reduction is supposed to be caused by a plastic strain increase at the crack tip which can blunt the crack tip (i.e., can reduce the local constraint due to the crack tip shape), and the transition from crack initiation to brittle fracture is governed by the notch radius and crack depth. Although the CWS is widely assumed to be a useful fracture index that is insensitive to the loading mode and initial crack depth, it might give unsafe predictions of fracture originating from shallow cracks. Therefore, a new framework considering the effect of plastic strain is necessary in seismic design to deal with brittle fracture during earthquakes.

This study applies a modified Weibull stress (MWS) approach [17–22] to evaluate the cleavage fracture criterion of structural steel considering that this evaluation is difficult using the conventional WS. The cleavage fracture criterion is then used for predicting brittle fracture during earthquakes. Because the effect of strain rate and plastic strain history are significant under earthquake, the MWS which was proposed by Bordet et al. [21,22] is applied in this study. Firstly, we introduce the MWS and evaluate the critical modified Weibull stress (CMWS) of cleavage fractures from shallow cracks by using the results of a low-temperature loading experiment and finite-element analysis (FEA). Next, the range of applications of the identified CMWS is investigated through the assessment of its dependency on the crack depth, strain rate, and prestrain. Finally, this paper applies the MWS-based approach to determine the critical fracture condition of a real structure model. Although, in a previous study [23], we have reported the applicability of this approach, in this paper we base on experimental and analytical data with higher reliability [24].

2. Modified Weibull stress (MWS)

2.1. Weakest link model considering microcrack initiation

The MWS proposed by Bordet et al. [21,22] incorporates a weakest link model considering the microcrack initiation process in ferrite crystal grains in steel. Microcracks in ferrite grains nucleate from cracked brittle particles (such as grain-boundary carbides, non-metallic inclusions, etc.) when crack tips in those particles reach adjacent ferrite matrices, and, as a result, possibly induce a cleavage fracture. In a weakest link model conventionally adapted to WS, the microcrack initiation is explicitly considered only at the onset of material yielding. However, in non-brittle materials such as steel, microcracks form under plastic deformation is a non-negligible since the number of cracked carbides increases with plastic strain. The microcrack initiation process depends also on the steel yield strength. Because of the temperature and strain rate dependency of the yield strength, microcracks tend to initiate heavily at low temperature and high strain rate. Meanwhile, the increase in the number of microcracks is supposed to decelerate after large plastic strain due to the reduction of the uncracked carbide population [21]. Bordet et al. [22] applied their weakest link model described below to fracture of steel in low temperature from $-196\,^{\circ}\mathrm{C}$ to $-100\,^{\circ}\mathrm{C}$, corresponding to the lower part of the ductile-brittle transition (DBT) curve.

In the weakest link model, the fracture process zone (FPZ) is divided into infinitesimal fracture volume units, and it is supposed that the fracture of one of the units would instantly result in a whole system fracture. Each unit possesses a potential trigger for cleavage fracture, and the probability of the local cleavage fracture, P_{cleav}, is defined for each unit. Bordet et al. [21] expressed P_{cleav} as the product of the probability of nucleating a microcrack and that of propagating the nucleated microcrack. Firstly, the increment of the probability of the local cleavage fracture, $\mathrm{d}P_{\mathrm{cleav}}$, is expressed as a function of the infinitesimal increment of equivalent plastic strain (hereafter written as plastic strain), $\mathrm{d}\varepsilon^{\mathrm{p}}$:

$$\mathrm{d}P_{\mathrm{cleav}} = p_{\mathrm{nucl}} p_{\mathrm{propag}} \mathrm{d}\varepsilon^{\mathrm{p}}, \tag{1}$$

where p_{nucl} and p_{propag} are, respectively, the local probability of nucleating a microcrack and propagating the nucleated microcrack (see their derivation in the next subsection). Next, P_{cleav} is written as the integral of $\mathrm{d}P_{\mathrm{cleav}}$ from 0 to the given plastic strain, $\varepsilon_{\mathrm{u}}{}^{\mathrm{p}}$:

$$P_{\mathrm{cleav}} = \int_0^{\varepsilon_{\mathrm{u}}^{\mathrm{p}}} p_{\mathrm{nucl}} p_{\mathrm{propag}} \mathrm{d}\varepsilon^{\mathrm{p}}. \tag{2}$$

Finally, on the basis of the assumption that the FPZ consists of n_{c} fracture volume units (weakest link theory), the fracture possibility of the whole FPZ, P_{f}, is

$$P_{\mathrm{f}} = 1 - \exp\left(- \sum_{i=1}^{n_{\mathrm{c}}} \int_0^{\varepsilon_{\mathrm{u}}^{\mathrm{p}}} p_{\mathrm{nucl},i} p_{\mathrm{propag},i} \mathrm{d}\varepsilon_i^{\mathrm{p}} \right), \tag{3}$$

since $P_{\mathrm{cleav},\,i} \ll 1$. Here, the subscript i denotes the i^{th} volume unit. The FPZ is assumed to be a plasticized part. P_{f}, evaluated in the FPZ at the tips of macroscale initial cracks, corresponds to the probability of brittle fracture in a structure.

2.2. Formulation of the MWS

p_{nucl} is derived as follows. Firstly, the relationship between the number of uncracked carbides, N_{unc}, yield strength, σ_{ys}, and a function to consider the dependency of the p_{nucl} on the plastic strain, $f(\varepsilon^{\mathrm{p}})$, ($f(\varepsilon^{\mathrm{p}}) = 1$ in studies by Bordet et al. [21,22]) can be written as

$$p_{\mathrm{uncl}} \propto N_{\mathrm{unc}}(\varepsilon^{\mathrm{p}})\, \sigma_{\mathrm{ys}}(T, \dot{\varepsilon})\, f(\varepsilon^{\mathrm{p}})\, \mathrm{d}\varepsilon^{\mathrm{p}}. \tag{4}$$

where T is the temperature and ε is the strain rate. Next, since the decrease in the number of uncracked carbides, $\mathrm{d}N_{\mathrm{unc}}$, is proportional to p_{nucl}, Eq. (4) gives

$$\mathrm{d}N_{\mathrm{unc}}(\varepsilon^{\mathrm{p}}) \propto -N_{\mathrm{unc}}(\varepsilon^{\mathrm{p}})\, \sigma_{\mathrm{ys}}(T, \dot{\varepsilon})\, f(\varepsilon^{\mathrm{p}})\, \mathrm{d}\varepsilon^{\mathrm{p}}. \tag{5}$$

Using the reference static yield strength, $\sigma_{\mathrm{ys},0}$, (at T_0, the reference temperature) and the reference plastic strain, $\varepsilon_0^{\mathrm{p}}$, Eq. (5) can be rewritten as

$$\mathrm{d}N_{\mathrm{unc}}(\varepsilon^{\mathrm{p}}) = -N_{\mathrm{unc}}(\varepsilon^{\mathrm{p}}) \frac{\sigma_{\mathrm{ys}}(T, \dot{\varepsilon})}{\sigma_{\mathrm{ys},\,0}} f(\varepsilon^{\mathrm{p}}) \frac{\mathrm{d}\varepsilon^{\mathrm{p}}}{\varepsilon_0^{\mathrm{p}}}. \tag{6}$$

Assuming that microcrack nucleation is possible as soon as plasticity occurs, N_{unc} can be expressed as:

$$N_{\mathrm{unc}}(\varepsilon^{\mathrm{p}}) = N_0 \exp\left(- \frac{\sigma_{\mathrm{ys}} \int_0^{\varepsilon^{\mathrm{p}}} f(\varepsilon^{\mathrm{p}}) \mathrm{d}\varepsilon^{\mathrm{p}}}{\sigma_{\mathrm{ys},\,0}\, \varepsilon_0^{\mathrm{p}}} \right). \tag{7}$$

Finally, replacing N_{unc} in Eq. (4) yields

$$p_{\mathrm{uncl}} \propto \frac{\sigma_{\mathrm{ys}}}{\sigma_{\mathrm{ys},0}\,\varepsilon_0^{\mathrm{p}}} f(\varepsilon^{\mathrm{p}}) \exp\left(-\frac{\sigma_{\mathrm{ys}}\int_0^{\varepsilon^{\mathrm{p}}} f(\varepsilon^{\mathrm{p}})\mathrm{d}\varepsilon^{\mathrm{p}}}{\sigma_{\mathrm{ys},0}\varepsilon_0^{\mathrm{p}}}\right)\mathrm{d}\varepsilon^{\mathrm{p}}. \tag{8}$$

When the strain at the stress peak in the initial crack tips is small enough and the effect of $\mathrm{d}N_{\mathrm{unc}}$ on p_{nucl} is negligible (i.e. if $\sigma_{\mathrm{ys},0}\cdot\varepsilon_0^{\mathrm{p}}/\sigma_{\mathrm{ys}} \ll \int_0^{\varepsilon^{\mathrm{p}}} f(\varepsilon^{\mathrm{p}})\mathrm{d}\varepsilon^{\mathrm{p}}$, as in situations investigated in this study, Eq. (8) can be simplified as

$$p_{\mathrm{uncl}} \propto \frac{\sigma_{\mathrm{ys}}}{\sigma_{\mathrm{ys},0}\,\varepsilon_0^{\mathrm{p}}} f(\varepsilon^{\mathrm{p}})\,\mathrm{d}\varepsilon^{\mathrm{p}}. \tag{9}$$

Meanwhile, similar to conventional WS, p_{propag} is formulated with the assumption of the Griffith's crack. However, considering that unstable crack propagation does not occur when the maximum principal stress is lower than a threshold critical stress, p_{propag} is given as:

$$p_{\mathrm{propag}}(\sigma_1) = \begin{cases} 0 & (\sigma_1 < \sigma_{\mathrm{th}}) \\ \left(\frac{\sigma_1}{\sigma_{\mathrm{u}}}\right)^m - \left(\frac{\sigma_{\mathrm{th}}}{\sigma_{\mathrm{u}}}\right)^m & (\sigma_1 \geqslant \sigma_{\mathrm{th}}) \end{cases}, \tag{10}$$

where σ_1 and σ_{th} are, respectively, the maximum principal stress and the threshold critical stress, the latter being a material constant. m and σ_{u} are also material constants corresponding to a shape and scale parameter in the conventional Weibull stress, respectively. σ_1 depends not only on the temperature and strain rate but also on the degree of constraint leading to fracture (such as initial crack depth, surface geometry of cracked part, loading mode, etc.). Note that, as Eq. (10) indicates, if $\sigma_1 < \sigma_{\mathrm{th}}$, p_{propag} becomes zero and $\mathrm{d}P_{\mathrm{cleav}}$ is then always zero for any p_{nucl}. As a result, the microcrack does not contribute to the cumulative fracture probability, P_{cleav}. This corresponds to when microcrack tips get blunt and are thus deactivated following stress reduction which causes a loss of strain rate hardening effect at the crack tips and, in turn, stops the dynamic propagation of the crack.

If the effect of $\mathrm{d}N_{\mathrm{unc}}$ on p_{nucl} is small enough, combining Eqs. (3), (9), and (10) leads to the following equation:

$$P_{\mathrm{f}} = 1-\exp\left(-\frac{1}{\kappa}\sum_{i=1}^{n_{\mathrm{c}}}\int_0^{\varepsilon_{\mathrm{u}}^{\mathrm{p}}} \frac{\sigma_{\mathrm{ys},i}}{\sigma_{\mathrm{ys},0}} f(\varepsilon_i^{\mathrm{p}}) \times \max\left(\frac{\sigma_{1,i}^m - \sigma_{\mathrm{th}}^m}{\sigma_u},\ 0\right)\mathrm{d}\varepsilon_i^{\mathrm{p}}\right), \tag{11}$$

where κ is a scaling constant. Since the number of initiation sites of cleavage fracture is proportional to the FPZ volume, V_{p}, Eq. (11) can be rewritten as

$$P_{\mathrm{f}} = 1-\exp\left\{-\frac{1}{\Sigma}\int_{V_{\mathrm{p}}}\left(\int_0^{\varepsilon_{\mathrm{u}}^{\mathrm{p}}} \frac{\sigma_{\mathrm{ys},i}}{\sigma_{\mathrm{ys},0}} f(\varepsilon_i^{\mathrm{p}}) \times \max\left(\frac{\sigma_{1,i}^m - \sigma_{\mathrm{th}}^m}{\sigma_u},\ 0\right)\mathrm{d}\varepsilon^{\mathrm{p}}\right)\frac{\mathrm{d}V}{V_0}\right\}, \tag{12}$$

where Σ and V_0 are scaling constants. Therefore, the MWS is defined as

$$\sigma_{\mathrm{w}}^* = \left\{\int_{V_{\mathrm{p}}}\left(\int_0^{\varepsilon_{\mathrm{u}}^{\mathrm{p}}} \frac{\sigma_{\mathrm{ys},i}}{\sigma_{\mathrm{ys},0}} f(\varepsilon_i^{\mathrm{p}}) \times \max\left(\frac{\sigma_{1,i}^m - \sigma_{\mathrm{th}}^m}{\sigma_u},\ 0\right)d\varepsilon_i^{\mathrm{p}}\right)\frac{\mathrm{d}V}{V_0}\right\}^{1/m}, \tag{13}$$

With $\sigma_{\mathrm{u}}{}^* = \Sigma^{1/m}$, Eq. (12) results in the standard equation of a two-parameter Weibull distribution:

$$P_f(\sigma_{\mathrm{w}}^*) = 1-\exp\left(-\left(\frac{\sigma_{\mathrm{w}}^*}{\sigma_{\mathrm{u}}^*}\right)^m\right). \tag{14}$$

m and $\sigma_{\mathrm{u}}{}^*$ are found to be a shape and scale parameter, respectively. Instead of using Eq. (14), the MWS is calculated numerically from the FEA results as follows:

$$\sigma_{\mathrm{w}}^* = \left(\sum_{j=1}^{n_e}\sum_{i=1}^{n_{\mathrm{IP},j}}\left(\sum_{l=1}^{n_l}\frac{\sigma_{\mathrm{ys},i}(T,\ \bar{\dot{\varepsilon}}_{i,j}(l))}{\sigma_{\mathrm{ys},0}} f(\varepsilon_{i,j}^{\mathrm{p}}) \times \max(\overline{\sigma}_{1,i,j}^m - \sigma_{\mathrm{th}}^m,\ 0)\Delta\varepsilon_{i,j}^{\mathrm{p}}(l)\right)\frac{V_{i,j}}{V_0}\right)^{1/m}, \tag{15}$$

where j denotes the j-th element ($1 \leq j \leq n_{\mathrm{e}}$), i is the number of Gauss points belonging to the j-th element ($1 \leq i \leq n_{\mathrm{IP},\,j}$), l denotes the number of load steps ($1 \leq l \leq n_l$), $\sigma_{\mathrm{ys}}(T,\ \bar{\dot{\varepsilon}}_{i,j}(l))$ denotes the yield strength at temperature T and averaged strain rate $\bar{\dot{\varepsilon}}_{i,j} = (\dot{\varepsilon}_{i,j}(l) + \dot{\varepsilon}_{i,j}(l-1))/2$, and $V_{i,\ j}$ is the volume of the j-th element. The averaged maximum principal stress is given as $\overline{\sigma}_{1,i,j} = (\sigma_{1,i,j}(l) + \sigma_{1,i,j}(l-1))/2$, and the formulation of $\sigma_{\mathrm{w}}{}^*$ in the case of a non-negligible reduction of N_{unc} is similarly done.

As seen above, the influence of the crack depth, surface geometry of the cracked part, loading mode, strain rate, and temperature are comprehensively considered in the calculation of the MWS. The CMWS is therefore assumed to be a unique characteristic of fracture resistance independent on those factors and thus potentially suited to assess the limit of brittle fracture during earthquakes.

3. Fracture limit evaluation based on modified Weibull stress

This chapter verifies the validity of the MWS approach in predicting brittle fracture during earthquakes through the application to a fracture in compact specimens, and derives the CMWS as a MWS-based fracture limit. The CMWS of the compact specimens is identified on the basis of low-temperature experiments and crack tip stress analysis. The applicability for predicting brittle fracture

from shallow cracks is then confirmed from the change in the MWS under loading.

3.1. Low-temperature experiments

In low-temperature experiments, the fracture limit in several conditions was experimentally obtained. By use of a FEA, two types of compact specimens, hereafter referred to as R0.5 and R5 series, were designed to reproduce the stress and strain state in the vicinity of the initial shallow crack tip that actually triggered a brittle fracture in the steel bridge pier during the Kobe earthquake [16]. As shown in Fig. 2, the R0.5 and R5 series differed by the radius of their respective notch, namely 0.5 and 5 mm, respectively. These notches generated a loaded condition with a corresponding weld bead toe radius, R_{toe}, at the tip of the initial crack made in the notches. The initial cracks simulating the shallow initial cracks in brittle fractures during earthquakes were high-cycle fatigue cracks of depth a_0, introduced by previously performed cyclic loading in elastic region. The specimens were respectively cut out of one of three target steels (structural hot-rolled 19 mm thick plates meeting Japan Industrial Standards) indicated in Table 1 so that the longitudinal direction corresponded to the rolling direction of these plates. SS400 was a mild steel with a ferrite-pearlite microstructure. SM490YB was a high-tensile steel made in a thermo-mechanical control process (TMCP) and with mainly a ferrite-pearlite microstructure. SM570Q was a high-tensile steel made through quench and tempering, and with mainly a bainite microstructure. The microstructure of each steel type is presented in Fig. 3. It was observed at a depth of a quarter of the plate thickness; the crack tip was located in this region.

The loading was implemented in a cooling bath filled with liquid nitrogen (-196 °C, lower shelf region of DBT curve) to simulate the lowest fracture toughness of weld toes when brittle fracture during earthquakes occurs under the significant fracture toughness reduction mainly due to seismic plastic strain history. The breaking took place in a quasi-static loading condition, and the critical load and displacement of each specimen were measured. Fig. 4 displays the experimental setup and Table 2 gives the measured critical load of several specimens, P_{cr}. All specimens showed a fracture surface consisting of clearly distinguishable two parts: a river pattern formed by cleavage fracture and a striation made by initial cracks.

To investigate higher fracture toughness, a similar experiment was carried out in a cooling bath filled with ethanol maintained at -100 °C (around the endpoint of lower shelf region of DBT curve). In this experiment, specimens with somewhat deeper initial cracks were employed because it was found out from preliminary experiments that brittle fractures of the target specimens at this temperature rarely occurred from cracks of thickness of lower than 1.5 mm. Table 3 shows the measured displacements. Since most of the specimens fractured after yielding, the results were represented by critical relative displacements between upper and lower fixtures, U_{cr}. There was variation in U_{cr} as shown in this table, yet all specimens presented a river pattern ~~and~~, no distinct stretch zone, and no clear evidence of ductile tearing at the end of the striation.

3.2. Crack tip stress analysis

In order to simulate each experiment and identify the local conditions around the crack tips, an FEA (using a commercial FEA software Abaqus) was implemented by considering the material, geometrical and boundary nonlinearities.

Fig. 5 presents an example of the finite element (FE) models employed in the analysis. Considering a finite sliding between the specimen and fixtures, the quarter region of the specimen and fixtures was modeled with a standard linear solid element. The crack surface was made by releasing the mirror symmetric conditions assigned to the center of the specimen and ensuring that the regions around a crack tip were divided in a large number of elements as shown in Fig. 5(b) and (c). Following the recommendation by Minami et al. [25], the minimum element length was 30 μm. The size of the elements around the notch bottom was determined on the basis of a confirmation of the calculation precision. In terms of material properties, the Young's modulus and Poisson ratio were assumed to be equal to 200 GPa and 0.3, respectively, and different stress-strain relationships were used depending on the steel type and experiment temperature, see Fig. 6. The stress-strain relationships at -100 °C, which show large plastic strain before fracture occurs, were obtained from tensile tests. By contrast, the curves at -196 °C correspond to an estimation through bending experiments

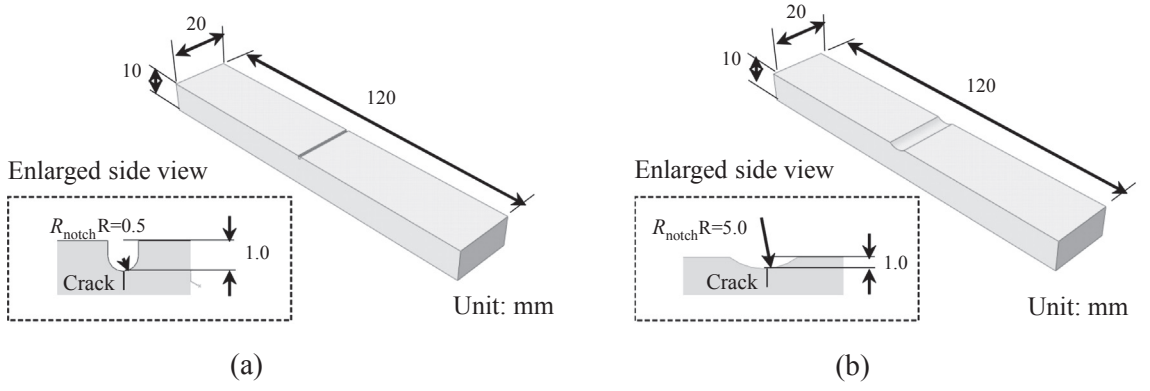

Fig. 2. Geometry and size of specimens with notches and shallow fatigue cracks: (a) R0.5 series; (b) R5 series.

Table 1
Mechanical capacity in room temperature and chemical composition of target steels.

Mechanical capacity test				Chemical composition [%]										Remarks
Yield strength [MPa]	Tensile strength [MPa]	Elongation [%]	Charpy value [J]	C × 100	Si × 100	Mn × 100	P × 1000	S × 1000	Ni × 100	Cr × 100	Mo × 100	Nb × 100	V × 100	
287	422	33	–	8	29	74	16	27	–	–	–	–	–	–
431	537	26	252	13	27	128	11	3	1	2	0	–	0	TMCP
595	664	36	305	10	23	153	8	2	1	2	0	3	6	Heat-treated

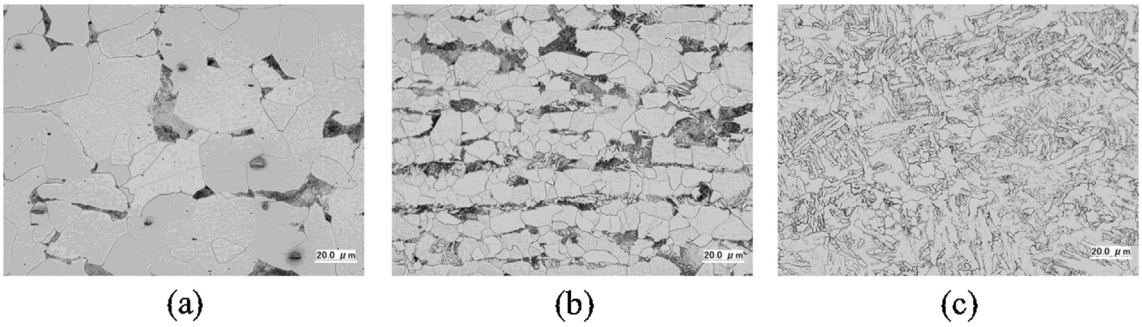

Fig. 3. Microstructure of each target steel: (a) SS400; (b) SM490YB; (c) SM570Q.

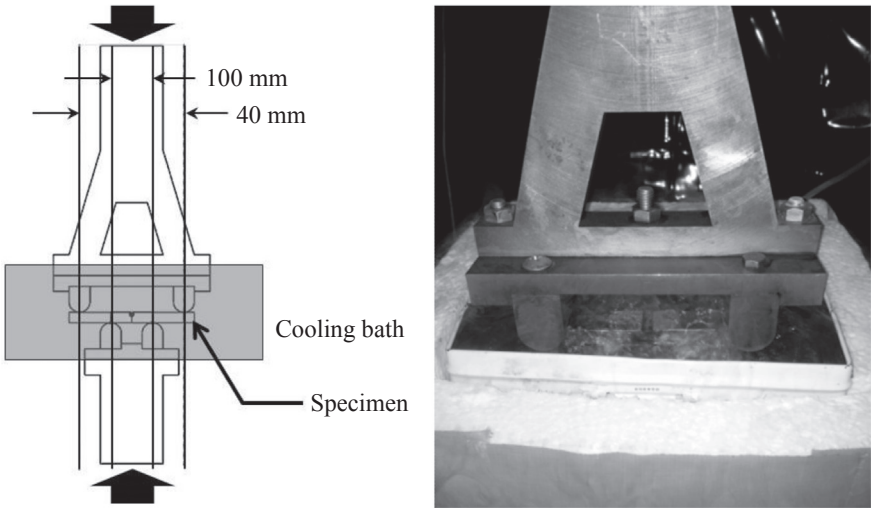

Fig. 4. Setup for low-temperature experiment to measure brittle fracture limit of each specimen.

Table 2
Measured critical load of each specimen in −196 °C.

SS400				SM490YB				SM570Q	
R05 series		R5 series		R05 series		R5 series		R05 series	
a_0	P_{cr}	a_0	P_{cr}	a_0	P_{cr}	a_0	P_{cr}	a_0	P_{cr}
0.43	11.48	0.52	12.65	0.36	23.09	0.30	21.24	0.36	13.79
0.56	10.48	0.61	13.70	0.42	21.16	0.34	21.12	0.42	13.73
0.69	8.68	0.62	12.23	0.52	16.69	0.49	15.83	0.51	13.94
0.75	8.79	0.69	9.89	0.57	18.22	0.68	18.64	0.56	14.16
0.80	9.90	0.74	11.02	0.62	17.55	0.73	18.24	0.63	13.97
0.83	8.77	0.76	13.21	0.64	15.91	0.84	15.31	0.70	12.01
0.97	9.43	0.87	9.63	0.65	15.42	0.94	16.81	0.87	11.55
1.04	8.42	1.09	11.54	0.67	16.33	1.12	14.23	0.95	11.34
1.07	8.27	1.10	9.32	0.73	15.01	1.16	13.49	1.05	15.46
1.08	9.66	1.16	8.24	0.87	13.20	1.18	15.84	1.06	11.48
1.12	8.91	1.19	7.49	0.96	13.16	1.22	18.48	1.07	10.38
1.23	9.60	1.32	8.42	1.07	13.03	1.30	12.47	1.18	10.82
1.26	8.09	1.88	6.03	1.26	12.28	1.60	10.20	1.36	9.92
1.72	6.62	2.11	5.89	1.28	14.22	2.71	9.30	1.80	10.16
2.33	7.36	2.20	6.68	1.77	10.68	3.34	9.05	2.00	8.98

a_0: initial crack depth [mm], P_{cr}: critical load [kN].

on notch-less specimens with the setup shown in Fig. 4. The loading was simulated with a vertical displacement of fixtures. The contact conditions between the specimen and fixtures were assumed to be a hard contact. The constraint was solved with the augmented Lagrange method with respect to the normal direction of the contact surface and accompanied by a friction force

Table 3
Measured critical displacement of each specimen in −100 °C.

SS400		SM490YB		SM570	
R05 series		R05 series		R05 series	
a_0	U_{cr}	a_0	U_{cr}	a_0	U_{cr}
1.45	0.95	1.76	4.35	1.53	8.90
1.53	1.55	1.89	2.51	1.57	8.41
1.59	1.52	1.98	2.11	1.72	3.53
1.68	1.23	2.06	4.31	1.83	1.37
1.85	2.25	2.17	6.36	1.87	1.71
1.91	1.99	2.25	1.84	2.07	1.19
1.97	2.18	2.29	3.81	2.09	1.45
2.18	2.48	2.30	2.94	2.12	1.22
2.20	1.79	2.33	1.78	2.20	2.91
2.27	2.72	2.36	2.18	2.23	1.73
2.30	0.65	2.44	2.63	2.34	0.90
2.31	1.93	2.47	6.26	2.53	1.10
2.34	4.42	2.69	3.48	2.58	1.20
2.38	1.88	2.96	5.35	2.63	1.03
2.45	0.95	–	–	2.65	0.91
–	–	–	–	2.68	0.88
–	–	–	–	2.84	0.95

a_0: initial crack depth [mm],
U_{cr}: critical disp. [mm]

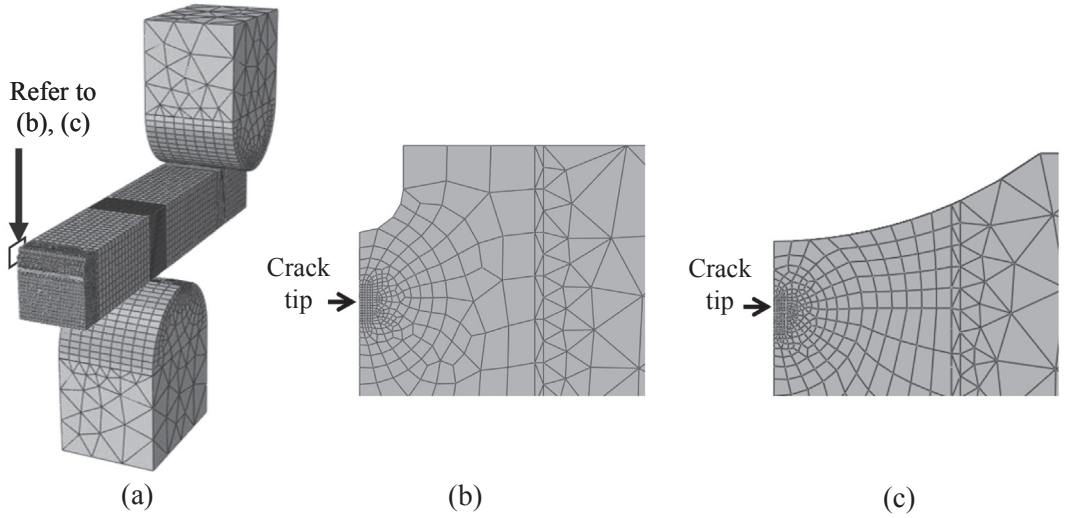

Fig. 5. Example of FE model used in the crack tip stress analysis: (a) whole view; (b) enlarged view of R0.5 series; (c) enlarged view of R5 series.

calculated by the Lagrange multiplier method. A friction coefficient of 0.21 was used. This value was obtained with a specimen without notch and initial crack in actual loading conditions as described in the previous section. The propagation of the initial crack was not considered in this analysis since stable propagation followed by cleavage fracture was negligible in the experiment.

3.3. Identification of the critical modified Weibull stress

The crack tip stress analysis revealed that ε_p at the peak position of σ_1 was less than 0.1 in every specimen at the fracture time. The effect of the reduction of N_{unc} with ε_p is supposed to be negligible [26,27] and Eq. (15), which ignores the effect of N_{unc}, was employed in the CMWS identification. Like Bordet et al. [21,22], the authors assumed that $f(\varepsilon_p)$ was equal to 1 in this section. The results of the simulating experiments conducted at −196 °C, in which a cleavage fracture was more dominant, were analyzed, and this, along with the least-square method, served as a basis for the estimation of the parameters m and σ_u^*. The permissible value of the relative error in m-updating was less than 1%. Following the method given by Bordet et al. [22], σ_{th} was determined to minimize the CMWS dependency on a_0 at −100 °C. The obtained parameters for each steel type are given in Table 4.

Fig. 7 shows the relationship between the CMWS and a_0 for each specimen, and also the CWS for SS400 at −196 °C (Fig. 7(a)). In

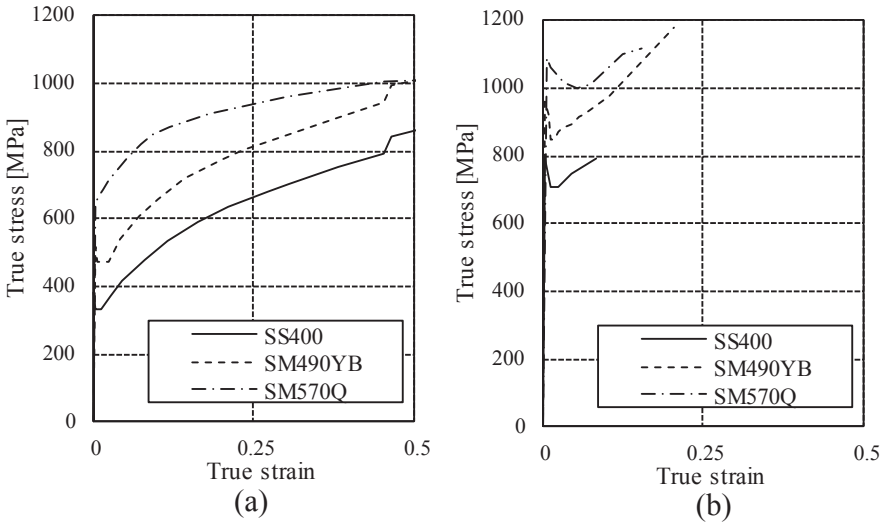

Fig. 6. Stress-strain relationships used in the crack tip stress analysis: (a) −100 °C; (b) −196 °C.

Table 4
Identified Weibull parameters and $\sigma_{th.}$

Steel type	m	σ_u^* [MPa]	σ_{th} [MPa]
SS400	37.24	1378	1250
SM490YB	43.21	1763	1275
SM570Q	37.06	1949	1790

each figure, three lines have been drawn on the basis of Eq. (14) and the assumption that all the experimentally obtained CMWS(P_f), or CWS(P_f), entirely followed a Weibull distribution. The three lines correspond to a fracture probability, P_f, of 0.05, 0.5, and 0.95, respectively. The results for SS400 (Fig. 7(a) and (b)) show smaller values of both the CMWS and the CWS for specimens with shallow cracks ($a_0 < 1$ mm) with respect to specimens with deeper cracks. The effect was more pronounced for the CWS, demonstrating the superiority of the CMWS as it was less sensitive to R_{notch} and a_0. The CMWS of the R0.5 series showed variance in Fig. 7(b), which corresponds to the variance of ε^p at the fracture time of several specimens. Fig. 7(b) and (c) show a dramatic temperature dependency of the CMWS, with significantly smaller CMWS values at −100 °C than at −196 °C. This is because the effect of larger ε^p values at the crack tips at the time of fracture at −196 °C was less significant than that of smaller σ_1 values at the crack tips, corresponding to the stress-strain relationships at this temperature (Fig. 6). This result implies that the temperature dependency of the microcrack nucleation and propagation process was not adequately considered in the calculations of the MWS.

Fig. 8 displays the MWS as a function of the loading point displacement for two different values of a_0. MWS monotonically increased for both tested specimens, and U_{cr} could thus be uniquely determined, in contrast to situations in which fracture occurs during a decrease of WS.

As observed above, with the assumption of $f(\varepsilon_p) = 1$, the R_{notch}- and a_0-dependency of fracture critical values, which was observed in the evaluation based on the WS, was reduced in the MWS-based evaluation. However, a temperature dependency of the CMWS was still identified, while the CMWS should be independent of temperature ideally. In order to obtain a temperature-independent CMWS, the MWS was partially redefined (see next section).

3.4. Redefinition of microcrack nucleation probability

In order to obtain a temperature-independent CMWS, the probability of microcrack nucleation was reevaluated. The fracture observation result by Kaechele and Tetelman [26], on which Bordet et al. [21,22] based their assumption $f(\varepsilon_p) = 1$, shows scattering, and the determination coefficient of the regression line, ${R_1}^2$ [28], shows low value: 0.612 at −196 °C, 0.016 at −180 °C, and 0.322 at −165 °C [23]. The form of p_{nucl} was then redefined here and it was investigated whether the temperature dependency of the microcrack nucleation and propagation was properly considered in the MWS so that it yielded a temperature-independent CMWS. Meanwhile, linear regression matches the results at room temperature [27].

As a possible modeling interpolating experimental results discussed above, we redefined $f(\varepsilon_p)$ as:

$$f(\varepsilon^p, T) = (\varepsilon^p)^{\alpha(T)}, \quad \alpha(T) = \frac{\alpha_0}{216}(20-T), \tag{16}$$

where α is the value of what is referred to here as plastic strain sensitivity and is not assumed to be a material parameter. It depends

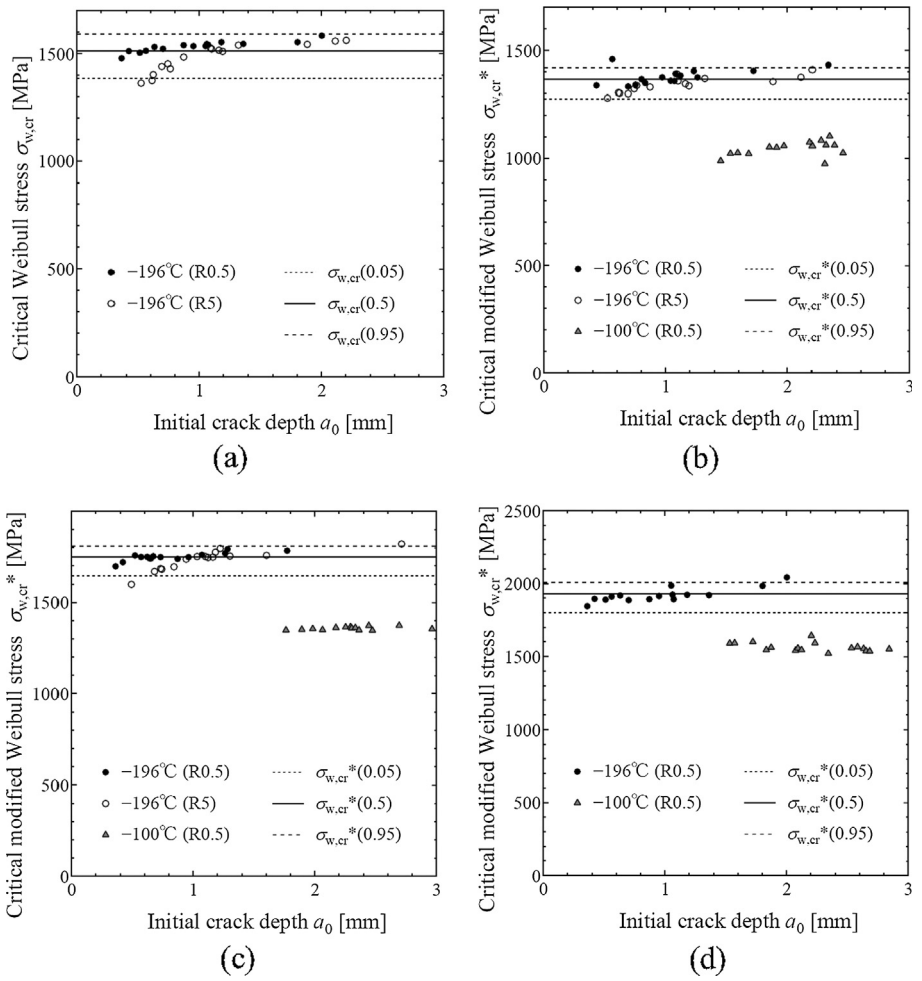

Fig. 7. Weibull stress and modified Weibull stress at the time fracture occurred: (a) CWS (SS400); (b) CMWS (SS400); (c) CMWS (SM490YB); (d) CMWS (SM570Q).

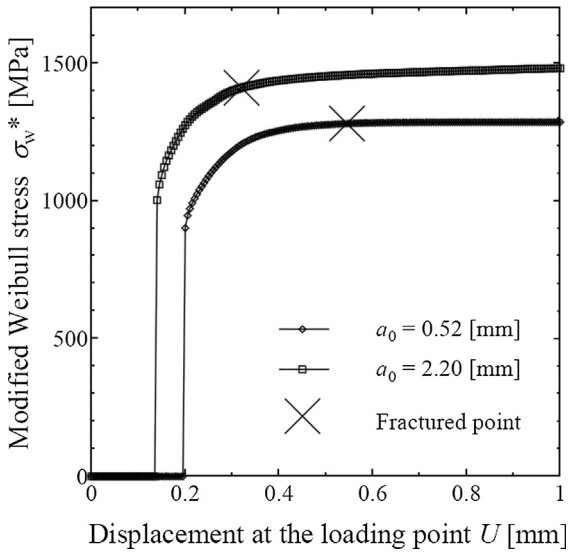

Fig. 8. Change of modified Weibull stress (SS400, R5, −196 ˚C).

on temperature: $\alpha = \alpha_0$ at −196 °C, and 0 at 20 °C; its value was obtained by a linear interpolation between these temperatures. The α_0 was assumed equal to 2 so that the temperature dependency of CMWS became negligible. Based on the redefined $f(\varepsilon_p)$, m, σ_u^* and σ_{th} were reevaluated from the procedure mentioned in the previous section.

The reevaluated MWS is shown in Fig. 9, and m, σ_u^* and σ_{th} are given in Table 5. In Fig. 9, the CMWS had similar values at both temperatures (−100 and −196 °C) for all types of target steel. It demonstrates that, by choosing an adequate combination of m, σ_u^* and σ_{th} for the MWS with α as defined in Eq. (16), the obtained MWS can be a brittle fracture index independent from a_0, R_{notch} and the temperature (namely fracture toughness level). As shown in Fig. 9 (d), the MWS-U relationship enabled an improved prediction of U_{cr} as a result of the monotonic increase of MWS with respect to U in the fracture region.

As shown in Table 5, m and σ_u^* were higher in SM490YB. Both are parameters related to the probability of microcrack propagation [21]. Therefore, it can be deduced that SM490YB exhibited a high microcrack propagation resistance, attributable to the fine granular structure obtained with TMCP. On the other hand, with a higher m, higher MWS and CMWS values were found for SM490YB (Fig. 9). This result interestingly corresponds to larger critical displacements (i.e. fracture toughness) experimentally measured with SM490YB compared to other types of steel. Therefore, the CMWS might be one of the indexes showing "true" fracture toughness–unlike the CWS and the critical crack-tip opening displacement, the CMWS is namely expected to be temperature- and strain-rate-independent.

The comparison between the microcrack nucleation behavior derived from Eq. (16) and the observation results reported by Kaechele and Tetelman [26] is shown in Fig. 10 where the vertical axis corresponds to the cumulative number of nucleated microcracks, and the horizontal axis to ε^P. The cumulative number of nucleated microcracks derived from Eq. (16) with the assumption of $\alpha_0 = 2$ and 0 (the latter corresponding to Bordet's model [21]) is displayed as curves of degree $\alpha+1$ and lines, respectively, and are also shown for comparison. Although the number of samples was not sufficient to evaluate the applicability of any of the above assumptions in a precise manner, the curves of degree $\alpha + 1$ showed a fair agreement with the experimental results at different temperatures.

The discussion above demonstrated that a MWS taking into account the observed microcrack nucleation behavior and the

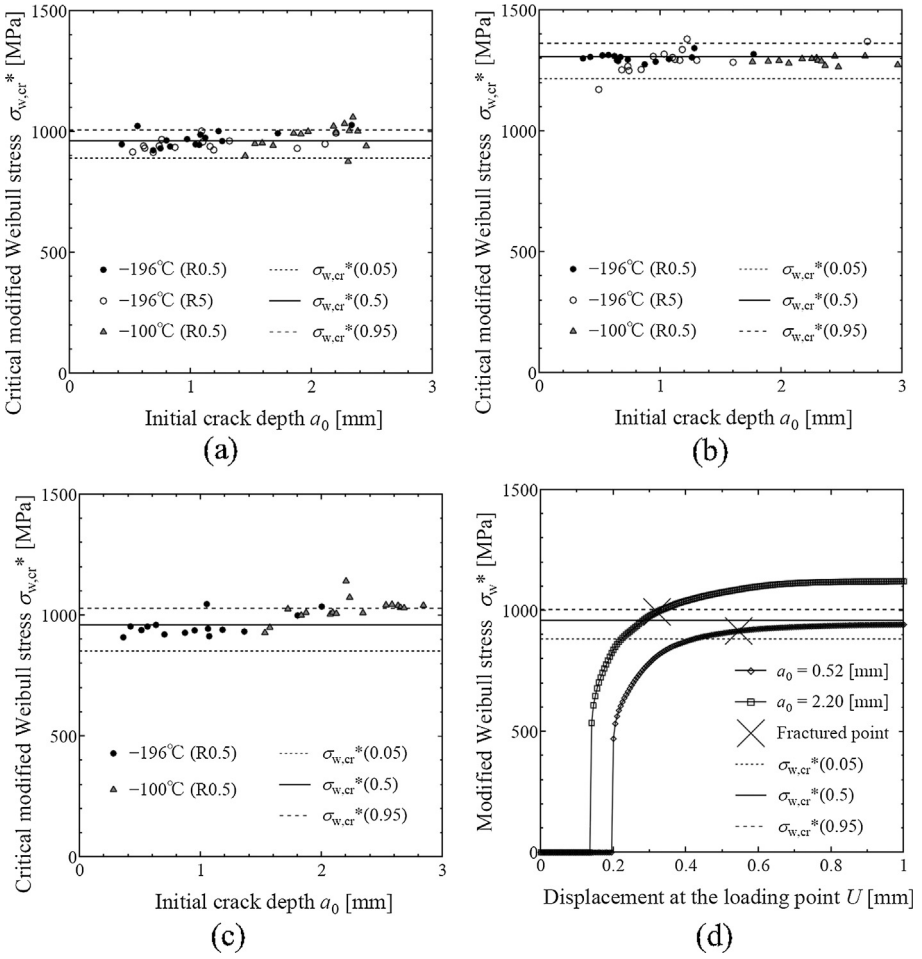

Fig. 9. Reevaluated modified Weibull stress at the time fracture occurred: (a) CMWS (SS400); (b) CMWS (SM490YB); (c) CMWS (SM570Q); (d) change of CMWS (SS400, R5, −196 °C).

Table 5
Reevaluated Weibull parameters and $\sigma_{th.}$

Steel type	m	σ_u^* [MPa]	σ_{th} [MPa]
SS400	32.84	972	1250
SM490YB	36.04	1320	1275
SM570Q	21.35	976	1960

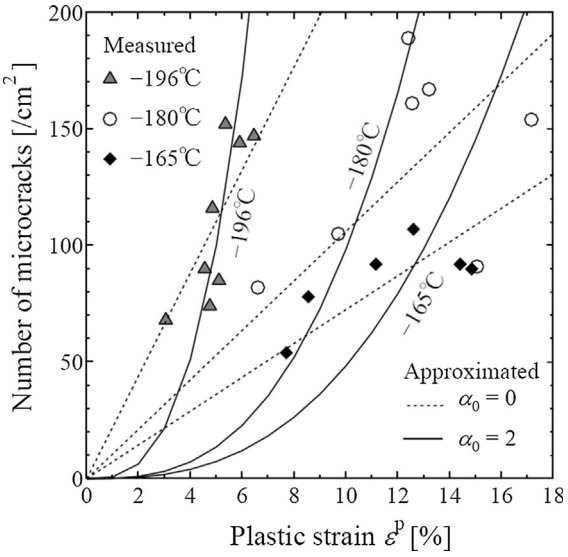

Fig. 10. Model of microcrack number increase in MWS-calculation.

conditions yielding a temperature-independent CMWS was derived through the redefinition of the microcrack nucleation probability model, $f(\varepsilon_p)$, on the basis of Eq. (16) with the assumption of $\alpha_0 = 2$. It also suggested an improved prediction of brittle fracture during earthquakes by using this MWS and the corresponding CMWS. Although further observation and statistical validation of the microcrack nucleation are still valid for reliability enhancement, in the following chapter, $\alpha_0 = 2$ was adopted in further investigations on the CMWS regarding its generality and applicability to fracture evaluation of a real structure.

4. Generality of critical modified Weibull stress

The MWS considered the effect on brittle fracture of some parameters such as initial crack depth, strain rate, etc. mainly in $\sigma_{ys,\,i}$ and $\sigma_{1,i}$ in Eq. (13) whereas parameters shown in Table 5 and the CMWS identified with these parameters were theoretically supposed to be a material constant independent from those effects. This chapter verifies this supposition through the examination of whether

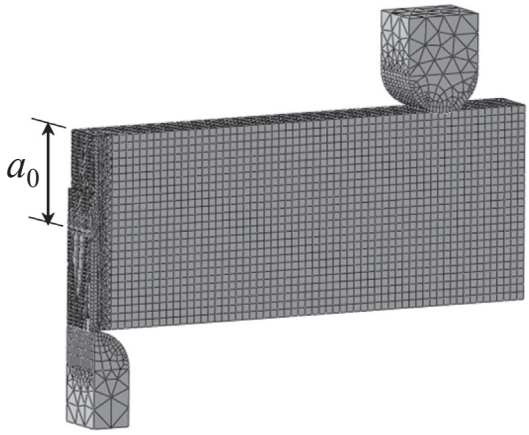

Fig. 11. FE model used in the analysis of CTOD test (thickness: 25 mm).

the dependency on the crack depth and strain rate of the experimentally measured critical CTOD were analytically reproduced in the predicted critical CTOD based on the MWS-based fracture evaluation. This chapter also addresses the effect of plastic strain history on the CMWS and evaluates the necessity of correction for tensile prestrain effects. The parameters identified in Section 3.4 were sequentially used in MWS-calculation in this chapter.

4.1. Crack depth independency

The CTOD test is one of the fracture toughness tests used for steel. In a CTOD test, the CTOD value measured at the instant of specimen fracture is defined as the critical CTOD, δ_{cr}, which is a characteristic value inherently depending on temperature, initial crack depth, loading speed and plastic strain history. This section evaluates the MWS during a CTOD test with FE simulation of a virgin material under quasi-static loading, and verifies whether the CMWS identified for specimens with shallow initial cracks is applicable to fracture prediction for CTOD specimens with deeper initial cracks through comparing the values of δ_{cr} obtained from the MWS-based fracture prediction and from measurement in the actual test.

In the FE simulation of the CTOD test, a quarter model shown in Fig. 11 was used. For the sake of comparison with actual measurements reported in WES2808 [15], the thickness was supposed to be 14 mm for SS400 and 25 mm for SM570Q, and the stress-strain relationships at −100 °C shown in Fig. 6(a) were used in the analysis.

According to the actual test conditions, the initial crack depth, a_0, was supposed to be equal to the thickness of each specimen, and a three-point bending was simulated. The other analytical conditions for crack and contact modeling were the same as those described in Section 3.2. The following equation was used for the estimation of the CTOD, δ, in the simulation:

$$\delta = \frac{K^2(1-\nu^2)}{2\sigma_{ys}(T)E} + \frac{r^p(W-a_0)V^p}{r^p(W-a_0) + a_0 + z}, \tag{17}$$

where K is the stress intensity factor; ν, the Poisson ratio; E, the Young modulus; V^p, the plastic component of the crack opening displacement (measured experimentally by clip gauges or determined by the node distance change in FEA); r^p, the rotation modulus (0.4); W, the width of the specimen (one-quarter length of the loading span); and z, the knife-edge height. When the MWS of the specimen was equal to the CMWS, $\sigma_{w,cr}{}^*$, the CTOD, δ, was supposed to be the critical CTOD, δ_{cr}. Three critical values of the CMWS, $\sigma_{w,cr}{}^*(0.05)$, $\sigma_{w,cr}{}^*(0.5)$ and $\sigma_{w,cr}{}^*(0.95)$, corresponding to P_f = 0.05, 0.5, 0.95, respectively, were used in the evaluation.

Fig. 12 compares the values of δ_{cr} estimated via the method described above and reported in WES2808 [15]. The smallest estimated δ_{cr} value was based on $\sigma_{w,cr}{}^*(0.05)$, while the largest was based on $\sigma_{w,cr}{}^*(0.95)$. As shown in Fig. 12(a), there is a good agreement between the estimation of δ_{cr} in SM570Q at −100 °C and the measured values in the same steel type. This strengthens the likelihood that the CMWS was independent from the initial crack depth and that the MWS-based fracture prediction could be applied to conventional brittle fractures initiating from deeper cracks. Fig. 12(b) displays the estimated and measured results obtained on two different types of steel but with a tensile strength of the same class. Both types of results were in the same order of magnitude. An enhanced agreement between estimated and measured values of the critical CTOD would be however expected when both types of values are obtained on the same steel type.

4.2. Strain rate independency

The results of the CTOD test conducted at 300 mm/s loading speed were compared with experimental results shown in WES2808 [15]. The dynamic implicit algorithm implemented in Abaqus was herein used in the simulation with a maximum time increment of

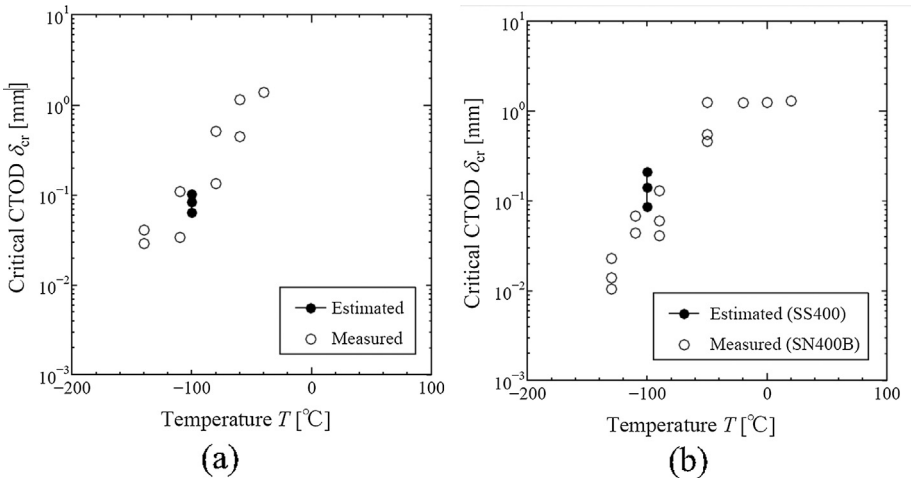

Fig. 12. Comparison of estimated values and measured values of the critical CTOD: (a) SM570Q (thickness: 25 mm); (b) 400 MPa-class steel (thickness: 14 mm).

1.0 μs. The strain rate dependency of the flow stress was considered by employing strain-rate-depending stress-strain relationships. These relationships are shown in Fig. 13(a) and were based on the prediction formula using the Arrhenius-type temperature dependency and the strain rate-temperature parameter R. The effect of heat generation on the flow stress was meanwhile ignored since an exploratory analysis estimated that the highest temperature rise at the crack tip under high speed loading up to fracture was about 5 °C in this specimen. In the MWS calculation with Eq. (15), the strain rate effect was taken into account via the strain-rate dependent yield stress. Therefore, the strain rate was considered in the CTOD test to affect not only the microcrack propagation behavior by using strain-rate dependent stress-strain relationships as a material property of each FE but also the microcrack nucleation behavior.

In Fig. 13(b), the MWS is plotted against the displacement as obtained from the simulation. Although fluctuation due to the impact-derived stress wave propagation is observed, the critical loading displacement, U_{cr}, was uniquely determined for the three CMWS values: $\sigma_{w,cr}^*(0.05)$, $\sigma_{w,cr}^*(0.5)$ and $\sigma_{w,cr}^*(0.95)$. The value of δ_{cr} eventually obtained on the basis of U_{cr} is presented in Fig. 14(a). The MWS-based δ_{cr} showed relatively high reproducibility of actually measured values in the same steel type and thickness, including dispersion. Additionally, the difference between the three estimated δ_{cr} values under quasi-static loading found in this and the previous section is relatively similar to the difference in the measured values; it represents the loading speed effects. This demonstrates the strain rate independency of the CMWS; the CMWS evaluated in a quasi-static experiment in the previous chapter was thus directly applicable to fracture estimation of the same type steel with high strain rate.

4.3. Prestrain independency

A CTOD test for steel with a uniform tensile prestrain of 10% under quasi-static loading is herein simulated and compared with data measured on WES2808 [15]. A static analysis as in Section 4.1 was then adopted and a stress-strain relationship reproducing the prestrain effect on the flow stress by expanding the initial yield surface with a plastic strain as high as 10% (Fig. 13(a)) was employed. In the MWS calculation, the initial value of $\varepsilon_{i,j}^{P}$ in Eq. (15) was set to 0.1, and the prestrain was considered to affect both the microcrack nucleation and propagation.

Fig. 14(b) displays the values of δ_{cr} determined from the MWS-U_{cr} relationships shown in Fig. 13(b). Although the estimated values of δ_{cr} were slightly lower than the measured ones, a similar difference between the estimated and measured values was shown in the results of virgin steel described in Section 4.1. These results indicate that the CMWS provided a proper prediction of fracture in target prestrained steel. The MWS-based approach has not heretofore been applied to the brittle fracture prediction of steel with plastic strain histories. These results however imply the possibility of a more universal prediction in which the same CMWS could be used for both virgin steel and steel with strain histories generated during earthquakes. Further research on steel with plastic strain history including compressive strain is needed to verify this possibility.

5. Attempt of fracture probability evaluation of a real structure

To illustrate the application of the MWS-based method to real structures, this chapter evaluates the critical condition of brittle fracture during earthquakes in a beam-to-column connection (BCC) of a steel bridge pier which corresponds to a type of road bridge piers (without any fillet on the BCCs) commonly found in Japan, and quantitatively determines the fracture probability focusing on the effect of the weld bead toe radius and initial crack depth at the fracture origin.

5.1. Target structure and initial crack

The target bridge pier is one of the most typical rigid-frame piers in Japan. Its composition in terms of beams, columns and BCCs,

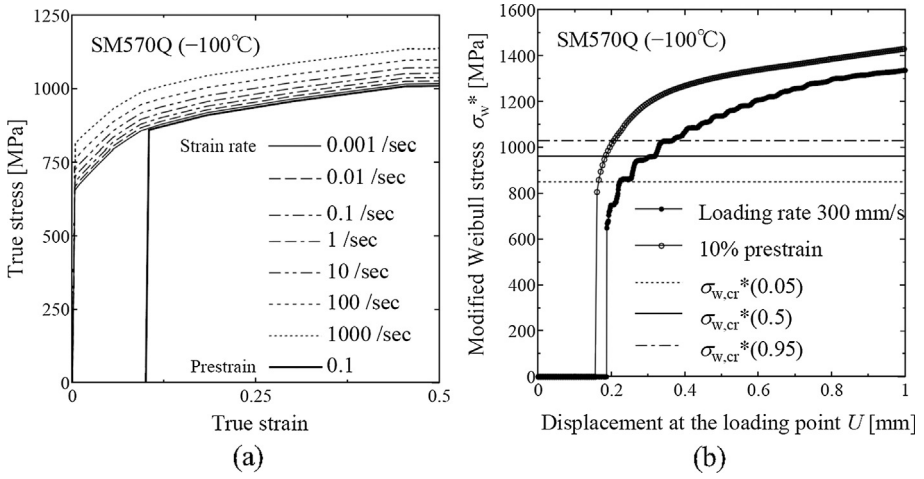

Fig. 13. Effects of strain rate and prestrain: (a) stress-strain relationships; (b) change of modified Weibull stress.

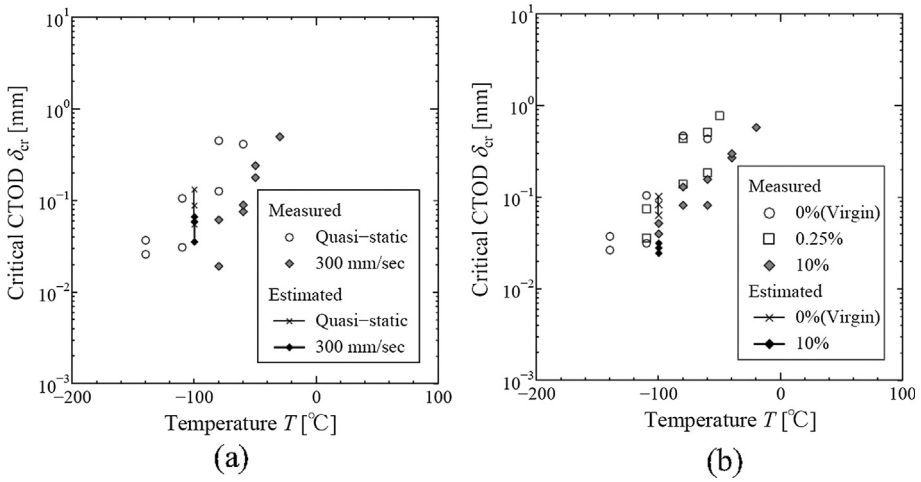

Fig. 14. Comparison of estimated values and measured values of the critical CTOD considering effects of strain rate and prestrain: (a) strain rate effect (SM570Q, thickness: 25 mm, −100 °C); (b) prestrain effect (SM570Q, thickness: 25 mm, −100 °C).

alongside the dimensions of the respective components, is shown in Fig. 15 (from Tamakoshi et al. [29]). In order to be able to employ material data, including the CMWS, it was assumed that only SS400 was used in the whole pier. The initial crack was assumed to be a semi-elliptical surface crack with an aspect ratio a_0/c_0 (a_0: depth, c_0: width) of 1/6. Three crack depths, a_0, were used: 0.5, 1.0, and 1.5 mm.

5.2. Analytical model and condition

On the basis of an actual damage situation (Fig. 1), the fracture origin was assumed to be located at the weld toe of one inside corner of a BCC, where the most significant plastic strain history occurs during earthquakes due to the superposition of the weld bead and BCC shape effect. The loading condition of the fracture origin therefore depends also on the deformation state of the pier. In light of this, an analysis considering both the global deformation of the pier and the local shape effect of the weld bead was herein implemented with a zooming method. Three FE models (whole pier model, BCC model and weld toe model) were used and are presented in Fig. 16.

The procedure of the zooming analysis consisted in:

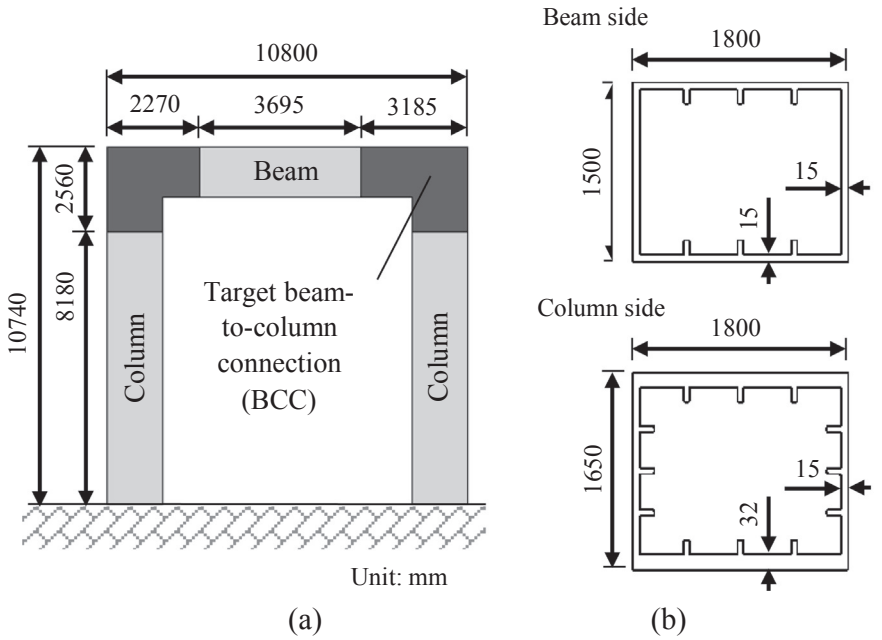

Fig. 15. Target steel bridge pier: (a) whole view; (b) section of BCC.

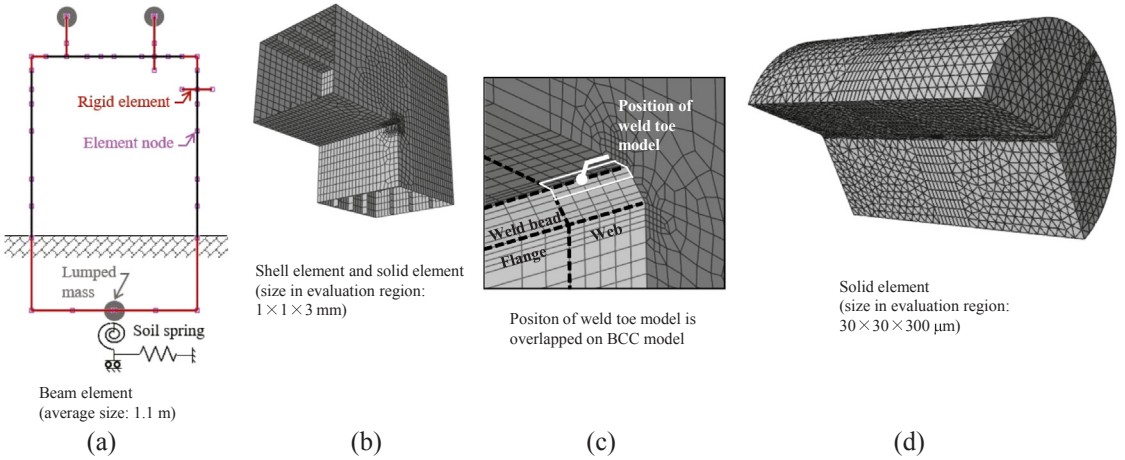

Fig. 16. FE models used in analysis of fracture origin of steel bridge pier BCC: (a) whole pier model; (b) BCC model; (c) view of around fracture origin; (d) weld toe model (R0.5).

(1) Obtaining the shape of the first natural vibration mode of the pier through eigenvalue analysis with the whole pier model. The dominant global pier deformation under earthquake loading was considered in this step.
(2) Reproducing the first mode shape in a static analysis with the BCC model, and applying the displacement to the edge surfaces of the BCC mode, which was proportional to the mode shape obtained in the previous step and was gradually increased (mode shape-based pushover analysis). The effect of the BCC and rough weld bead shapes was considered in this step.
(3) Transferring the displacement of the BCC model analysis to the weld toe model analysis (second zooming). In this zooming, the submodeling function in Abaqus was used. The FE nodes on the edge surface of the weld toe model were moved to the corresponding nodes in the BCC model. The effect of the weld bead shape including the toe radius was eventually considered here.

This procedure is described more circumstantially in Tamura et al. [30].

In this study, the material properties of SS400 were used and the initial crack was initially included in the weld toe model. The crack tip region of the model was divided into FEs with a minimum length of 30 μm, as displayed in Fig. 17. In order to investigate the effect of the weld toe radius, R_{toe}, on the brittle fracture condition of the BCC, nine weld toe models were implemented with three different toe radii (0.25, 0.5 and 5 mm) and crack depths (0.5, 1.0 and 1.5 mm). Hereafter, each model is referred to as the letter R followed by the toe radius and crack depth, for instance R0.25–0.5 for $R_{toe} = 0.25$ mm and $a_0 = 0.5$ mm. The R_{toe} values of 0.25 and 0.5 mm corresponded to as-welded toes, while that of 5 mm to typical finished weld toes. Although the strain concentration on finished weld toes is small, it was considered that large earthquakes lasting for a long time, such as the Tohoku earthquake in 2011, might cause brittle fracture through long plastic strain histories. By supposing that the welding heat, high strain rate and severe plastic strain histories widely reduced the fracture toughness of the weld toe, the stress-strain relationship at −100 °C presented in Fig. 6 was assigned to the whole set of weld toe models in order to reproduce the low fracture toughness condition. Also, a temperature of −100 °C was assumed in the MWS calculation.

It is desirable to first set the initial fracture toughness distribution and then evaluate the MWS using the plastic strain and strain rate at integration points in each FE as done in Sections 4.2 and 4.3. However, since the CMWS distribution and influence of more complex plastic strain histories on the MWS in weld parts are still unknown, we herein considered a situation where the fracture

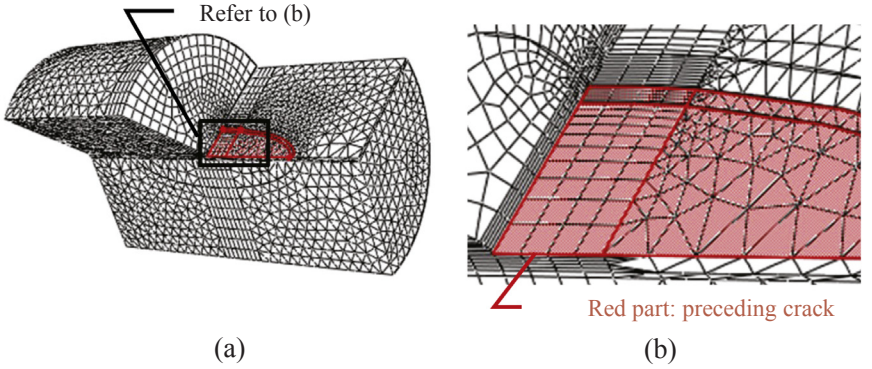

Fig. 17. Preceding crack and elements at the crack tip (R0.5–0.5): (a) whole view (1/4 of near side is hidden); (b) zoom-up view around preceding crack.

toughness in the vicinity of an initial crack tip (i.e. the FPZ) was uniform. The existing approach described in WES2808 [15] was adopted. It consists in cutting a specimen from the target and controlling the fracture toughness by changing the temperature uniformly. Similarly to this approach, the applicable range was limited here to cases in which the fracture toughness distribution at the crack tip vicinity could be regarded as uniform. However, in contrast to the existing approach, the effect of the weld part shape (including the weld toe radius considered here) was estimated analytically.

5.3. Relationship between brittle fracture limit and weld toe radius

Fig. 18 presents the first mode shape of the in-plane deformation obtained using the whole pier model. Gauge points of the BCC displacement, Δ, defined by the change in the distance between the edges of the BCC, were used to evaluate the degree of deformation of the whole BCC. By comparing these results with those using the BCC model giving perfect elastic material properties, a yield BCC displacement of the target (denoted Δ_y) of 0.55 mm was found.

The MWS was evaluated as a function of Δ using the results obtained with the weld toe models and parameters identified in Section 3.4. In Fig. 19, the corresponding MWS was plotted against normalized displacement, Δ/Δ_y. It can be seen that a smaller toe radius and larger crack depth led to higher values of the MWS for shallow initial cracks.

The results of the evaluation of the critical BCC displacement, Δ_{cr}, on the basis of the CMWS corresponding to Δ when the MWS exceeds $\sigma_{w,\,cr}{}^{*}(0.05)$ are presented in Fig. 20. The plots showing Δ_{cr} for the R0.25 series indicate that the critical BCC displacement, Δ_{cr}, decreases with increasing crack depth (a_0). Besides, by comparing the R0.25, R0.5 and R5 series at the same a_0, it was found that the shallower the initial crack depth was, the more significant the influence of R_{toe} was. It is conceivable that the actual Δ_{cr} of the R5 series was higher because their strain rate and plastic strain history were smaller than for the other series.

As demonstrated above, by applying the MWS to the evaluation of the critical condition for brittle fracture during earthquakes, it was analytically possible to consider the difference of constraint at the shallow crack tip, while it cannot be estimated by existing approaches based on experiments. As a result, the effect of R_{toe} on the fracture limit was quantitatively evaluated.

The MWS-based approach applied in this chapter has the potential to be extended to a wider range of applications through further research. For that purpose, surveys on the initial fracture toughness distribution in actual weld parts, fracture toughness deterioration due to strain rate and cyclic plastic strain histories, and temperature rise distribution caused by plastic deformation are recommended.

6. Conclusion

Brittle fracture during earthquake can also originate from shallow initial cracks of depth less than 1 mm. In order to establish the evaluation methodology of the critical condition of brittle fracture during earthquakes originating from shallow microcracks, this study introduced a modified Weibull stress (MWS) which considered the process of microcrack nucleation and propagation. This study further implemented fracture experiments and finite-element analyses of three types of structural steels. The generality of the obtained critical MWS (CMWS) was then verified in terms of the initial crack depth, strain rate and prestrain. Moreover, the fracture probability of a real structure with a significantly reduced fracture toughness at the fracture origin was estimated. The results are summarized as follows:

Through a redefinition of the microcrack nucleation probability, the CMWS was almost independent of temperature, initial crack depth and notch radius, the latter reproducing the weld toe radius effect. It was possible to determine the CMWS in target specimens designed to reproduce the condition of one of the actual origins of brittle fracture during earthquakes. The evaluated MWS showed a

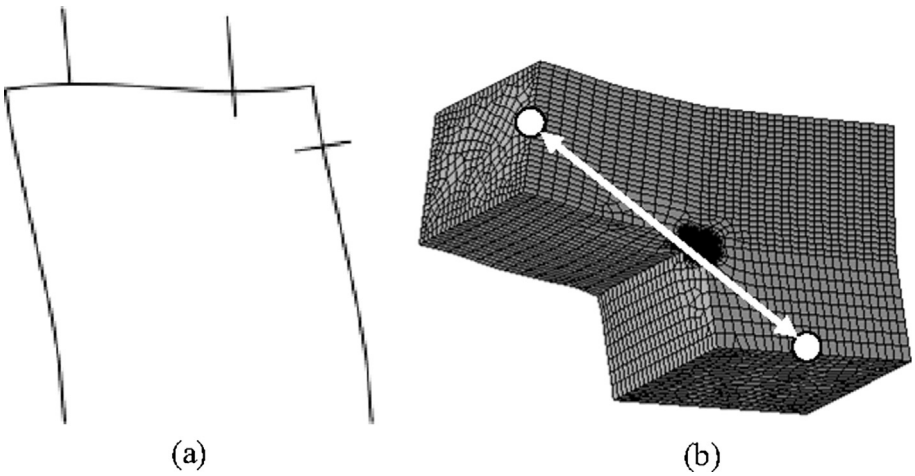

Fig. 18. Assumed seismic deformation of the pier and gauge points of BCC displacement: (a) in-plane 1st mode shape (dominant seismic mode); (b) gauge points of BCC displacement.

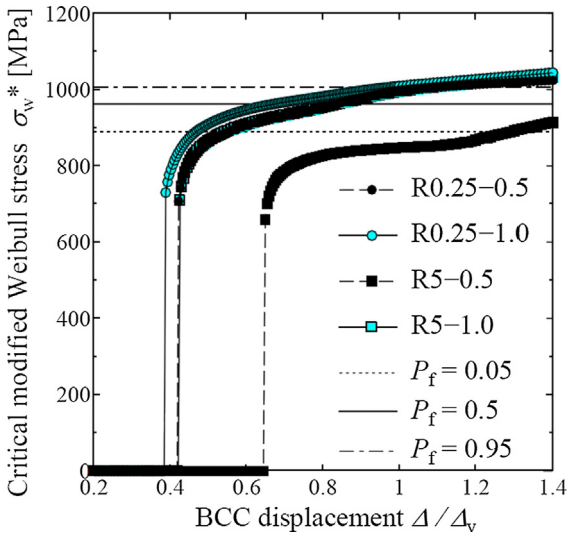

Fig. 19. MWS change in BCC with each preceding crack.

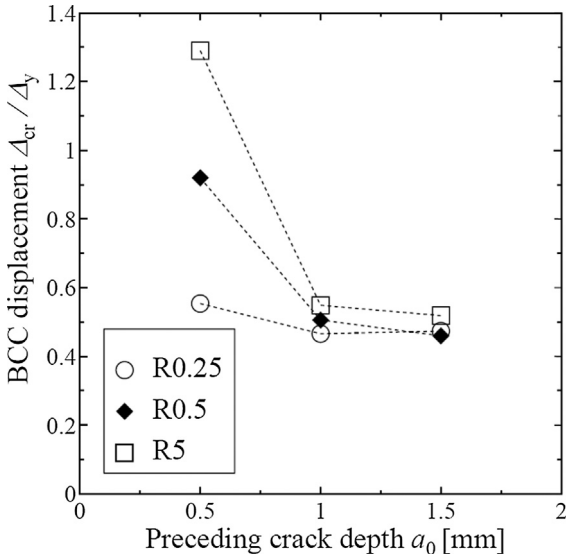

Fig. 20. Critical BCC connection corresponding to fracture probability of 5%

monotonic increase allowing the specification of the critical displacement of the loading point. The MWS was demonstrated to be an adequate index also in the case of fractures originating from shallow initial cracks.

The critical condition was estimated through a CTOD test based on the MWS, and it was shown that the dependency of the identified CMWS on the initial crack depth was small. The MWS-based fracture prediction was applicable to conventionally targeted fractures occurring from deeper initial cracks. Moreover, in the CTOD test condition reported in WES2808 [15], the independency of the CMWS from strain rate and prestrain was assumed in this study.

The fracture prediction in a beam-to-column connection (BCC) of a steel bridge pier, as an example of practical application, demonstrated that the MWS-based approach quantitatively clarified the influence of the weld toe radius and initial crack depth at the fracture origin on the critical BCC displacement.

From these results, it can be concluded that the introduction of the MWS made prediction of brittle fracture during earthquakes effectively feasible owing to the high generality of the CMWS. The fact that a unique CMWS could be applied to different temperature, strain rate and prestrain conditions interestingly suggests that the CMWS might be a more general fracture toughness index that is independent of these factors.

Acknowledgments

This work was supported by JSSC Grant for research on steel structures (2010), Johs. I. Svanholms Fond Grant for Steel Structure Research and Education Assistance Project (2013) and JSPS KAKENHI Grant (Nos. 11J00061 and JP25820199).

References

[1] Watanabe E, Maekawa Y, Sugiura K, Kitane Y. Damages and seismic performance of steel bridges. JSCE Mag Civil Eng 1995;80(8):54–62. [in Japanese].
[2] Miller DK. Lessons learned from the Northridge earthquake. Eng Struct 1998;20(4–6):249–60.
[3] Mahin SA. Lessons from damage to steel building during the Northridge earthquake. Eng Struct 1998;20(4–6):261–70.
[4] Kuwamura H, Yamamoto K. Ductile crack as trigger of brittle fracture in steel. J Struct Eng 1997;123(6):729–35.
[5] Tamura H, Sasaki E, Kim S, Yamada H, Katsuchi H. Weld shape effect on ductile crack initiation in weld joints subjected to seismic bending and control effect by toe grinding. Steel Constr Eng 2010;17(68):55–68. [in Japanese].
[6] Tamura H, Sasaki E, Yamada H, Katsuchi H. Analytical study focusing on stress triaxiality on factor of brittle fracture during earthquakes in steel bridge bents. J Jpn Soc Civil Eng Ser A 2010;66(3):420–34. [in Japanese].
[7] Sakano M, Mikami I, Takaba S. Low cycle fatigue behavior of steel pier beam-column joint. J Jpn Soc Civil Eng 1997;1997(563/I-39):49–60. [in Japanese].
[8] Sasaki E, Arakawa Y, Miki C, Ichikawa A. Low cycle fatigue cracks occurred at weld toe if ribs and possibility of occurrence of brittle fracture from them. J Struct Eng 2002;48A:1107–12. [in Japanese].
[9] Tateishi K, Hanji T, Minami K. A prediction model for extremely low cycle fatigue life under variable strain amplitude. J Jpn Soc Civil Eng 2004(733/I-69):149–58. [in Japanese].
[10] Miki C, Sasaki E, Kyuba Y, Takenoi I. Deterioration of fracture toughness of steel by effect of tensile and compressive prestrain. J Jpn Soc Civil Eng 2000;2000(640/I-50):165–75. [in Japanese].
[11] Sasaki E, Arakawa Y, Miki C, Ichikawa A. Required fracture toughness of steel to prevent brittle fracture during earthquakes in steel bridge piers. J Jpn Soc Civil Eng 2003(731/I-63):93–102. [in Japanese].
[12] Toyosada M, Gotoh K, Sagara K. J Soc Naval Archit Jpn 1991(170):651–63. [in Japanese].
[13] Onishi T, Sasaki E, Tamura H, Yamada H, Katsuchi H. Study on level and effect of local temperature rise due to plastic deformation of steel frame bridge. J Jpn Soc Civil Eng Ser A1 2013;69(2):361–71. [in Japanese].
[14] Beremin FM. A local criterion for cleavage fracture of a nuclear pressure bessel steel. Metall Trans A 1983;14A:2277–87.
[15] WES2808. The Japan Welding Engineering Society: method of assessing brittle fracture in steel weldments subjected to large cyclic and dynamic strain; 2003.
[16] Tamura, H., Sasaki, E., Yamada, H., Katsuchi, H., 2012. Effect of weld bead shape on critical Weibull stress for initiation of brittle fracture during earthquakes. In: Proceedings of the 4th international conference on computational methods, gold coast.
[17] Kroon M, Faleskog J. A probabilistic model for cleavage fracture with a length scale-influence of material parameters and constraint. Int J Fract 2002;118:99–118.
[18] Faleskog J, Kroon M, Öberg H. A probabilistic model for cleavage fracture with a length scale-parameter estimation and predictions of stationary crack experiments. Eng Fract Mech 2004;71:57–79.
[19] Gao X, Zhang G, Srivatsan TS. Prediction of cleavage fracture in ferritic steels: a modified Weibull stress model. Mater Sci Eng A 2005;394:210–9.
[20] Gao X, Zhang G, Srivatsan TS. A probalistic model for prediction of cleavage fracture in the ductile-to-brittle transition region and the effect of temperature on model parameters. Mater Sci Eng A 2006;415:264–72.
[21] Bordet SR, Karstensen AD, Knowles DM, Wiesner CS. A new statistical local criterion for cleavage fracture in steel. Part I: model presentation. Eng Fract Mech 2005;72:435–52.
[22] Bordet SR, Karstensen AD, Knowles DM, Wiesner CS. A new statistical local criterion for cleavage fracture in steel. Part II: application to an offshore structural steel. Eng Fract Mech 2005;72:453–74.
[23] Tamura H, Sasaki E. A study on modified Weibull stress based evaluation of brittle fracture occurrence during earthquakes in steel members. J Jpn Soc Civil Eng Ser A1 2015;71(2):173–85. [in Japanese].
[24] Tamura H, Tominaga S, Sasaki E. Fracture toughness evaluation of structural steel based on modified Weibull stress. Steel Constr Eng 2016;24:620–7. [in Japanese].
[25] Minami F. Fracture assessment method using the Weibull stress-Part I (review). J Jpn Weld Soc 2006;75(5):416–46. [in Japanese].
[26] Kaechele LE, Tetelman AS. A statistical investigation of microcrack formation. Acta Metall 1969;17:463–75.
[27] Gurland J. Observations on the fracture of cementite particles in a spheroidized 1.05% C steel deformed at room temperature. Acta Metall 1972;20:735–41.
[28] Kvålseth TO. Cautionary note about R2. Am Stat 1985;39(4, Part 1):279–85.
[29] Tamakoshi, T., Nakasu, K., Ishio, M., Kinouch, K., 2006. Study on fatigue design method for the beam-to-column connections of steel piers of highway bridges–examination of analytical method using “the constant shear flow panels. Technical note of national institute for land and infrastructure management, No. 296 [in Japanese].
[30] Tamura, H. Nomura, K. and Ikeda, K., 2013. Sensitivity analysis on strain concentration. In: 21st JSSC proceedings, pp. 777–784 [in Japanese].